Research Article Vol. 30, No. 12 / 6 Jun 2022 / Optics Express 20389
Optics EXPRESS

Generation of 2D Airy beams with switchable metasurfaces

XIAOJU XUE,[1] BIJUN XU,[1,2,*] BAIRUI WU,[1] JINGWEI LIN,[3] XIAOGANG WANG,[1] XINNING YU,[1] LU LIN,[1] AND HONGQIANG LI[2,4]

[1]School of Science, Zhejiang University of Science and Technology, Hangzhou, China
[2]Institute of Dongguan-Tongji University, Dongguan, Guangdong 523808, China
[3]College of Electrical and Information Engineering, Hunan University, Changsha, China
[4]School of Physics Science and Engineering, Tongji University, Shanghai 200092, China
*xubijun@zust.edu.cn

Abstract: Airy beams exhibit intriguing characteristics, such as diffraction-free propagation, self-acceleration, and self-healing, which have aroused great research interest. However, the spatial light modulator that generates Airy beams has problems such as narrow operational bandwidth, high cost, poor phase discretization, and single realization function. In the visible region (λ~532 nm), we proposed a switchable all-dielectric metasurface for generating transmissive and reflective two-dimensional (2D) Airy beams. The metasurface was mainly composed of titanium dioxide nanopillars and vanadium dioxide substrate. Based on the Pancharatnam-Berry phase principle, a high-efficient Airy beam can be generated by controlling the phase transition of vanadium dioxide and changing the polarization state of the incident light. The optimized optical intensity conversion efficiencies of the transmissive and reflective metasurfaces were as high as 97% and 70%, respectively. In the field of biomedical and applied physics, our designed switchable metasurface is expected to offer the possibility of creating compact optical and photonic platforms for efficient generation and dynamic modulation of optical beams and open up a novel path for the application of high-resolution optical imaging systems.

1. Introduction

As known to all, optical beams have diffractive properties. However, the energy of an optical beam propagating in free space disperses gradually with the increase of propagation distance, and the light spot expands from inside to outside, which may be detrimental to the application in optical communication and military technology. As a result, people are eager to find a new solution, namely diffraction-free beam. The most representative diffraction-free beam propagating along a straight line is the Bessel beam [1], while a popular diffraction-free beam is the Airy beam in recent years, which is also a representative form of accelerating beams [2]. The Airy beam is a diffraction-free beam propagating along a curved path in free space with an amplitude intensity satisfying the parabolic trajectory generated by the horizontal motion of particles under the influence of gravity. In 1979, Berry and Balazs theoretically demonstrated the particular solution to one-dimensional Schrödinger equation — the Airy function, which implied particles and waves carried infinite energy [3]. In 2007, Siviloglou and his students introduced finite energy Airy beams through theoretical derivation and experimental demonstration [4]. Generally, many devices have been developed to generate Airy beams, such as spatial light modulators (SLMs) for cubic phase modulation of beams [5–7], transmissive liquid crystals [8,9]. These optical devices have large bulk, high investment costs, and generate wide Airy beams with fixed non-diffractive propagation distances, so they are not applicable in optical imaging, Airy surface plasma excitations, lasers, and light bullets scenarios. So far, the plasmonic and dielectric metasurfaces have driven the field of photonics in a more far-reaching direction, and multifunctional ultrathin optical devices composed of them hold strong promise for applications

#460193 https://doi.org/10.1364/OE.460193
Journal © 2022 Received 6 Apr 2022; revised 13 May 2022; accepted 13 May 2022; published 23 May 2022

Optics EXPRESS

in electron beams [10], high-resolution optical microscopes [11], and optical manipulation of biological cells [12].

Corresponding to the 2D structure of metamaterials [13], the electromagnetic metasurface is a planar functional device composed of subwavelength metal or dielectric materials. It is able to dynamically modulate the amplitude, phase, and polarization modes of the incident light on nanostructures, thus attracting attentions from a large number of researchers [14–18]. In recent years, pure phase modulation or complex amplitude modulation of the incident wavefront based on the metasurface has been continuously implemented to generate Airy beams, and significant progress has been made in the fields of nonlinear optics [19] and surface plasma optics [20]. However, due to the limitations of fixed wavelengths and periods arising from the design of the unit cell and the inability to cover the entire phase range of 0 to 2π with phase delay for scattered light, the metasurface-based modulation usually turns out with low metasurface transmittance or reflectance. Then functionally multiplexed metasurface devices were developed [21–25], but the increased functionality has also given rise to higher design complexity and lower flexibility of the wavefront modulation function. The implementation of highly efficient transmissive, functionally switchable, and structurally simple metasurface has become a driving force for subsequent and continuous exploration.

In this paper, we proposed a switchable dielectric metasurface for generating 2D Airy beams in the visible range. The metasurface was composed of an array of titanium dioxide nanopillars, with a substrate of silicon dioxide and vanadium dioxide. By the principle of Mie, TiO_2 possesses high refractive index, low loss, and high coupling degree with light, which are exploitable advantages for generating high-efficiency Airy beams. According to the geometric phase method and the characteristics of the phase change material, the metasurface generates transmissive 2D Airy beams with high polarization conversion efficiency and energy absorption when VO_2 is in the insulating phase. The VO_2 turns into the metallic phase when the surrounding temperature exceeds the phase transition temperature. Then the operating mode of the metasurface changes to produce a same reflective Airy beam as the transmissive metasurface. The simulation results showed that the optical intensity conversion efficiencies of the transmissive and reflective metasurfaces were 97% and 70%, respectively. The metasurface demonstrated significant advantages, such as ultra-thinness, small size, dynamically switchable functionality, and high efficiency, over conventional methods of generating Airy beams with spatial light modulators. In contrast to the previously reported research work [26–31], we further compared the effects of different wavelengths and polarization states of incident light on the metasurface, thus confirming the broadband characteristics and flexibility of our designed metasurface.

2. Structure description and method

By principle [2], the electric field envelope of finite energy Airy beams can be formularized as

$$\Phi(\xi, x) = Ai\left[bx - \left(\frac{\xi}{2}\right)^2 + ia\xi \ \right] exp\left[\ ax - \frac{a\xi^2}{2} - i\frac{\xi^3}{12} + i\frac{a^2\xi}{2} + i\frac{x\xi}{2}\right] \tag{1}$$

Similarly, according to the optical paraxial wave equation, the transverse field distribution of the 2D Airy wave packet is formulated as follows [32]:

$$\Phi(x, y, z = 0) = Ai\left(\frac{x}{x_0}\right)\exp\left(\frac{ax}{x_0}\right) Ai\left(\frac{y}{y_0}\right)\exp\left(\frac{ay}{y_0}\right) \tag{2}$$

where Ai is the Airy function; a is the truncation factor of the Airy beams, here set to 0.05; b is the transverse scale; x represents the transverse coordinate; $\xi = \frac{z}{kx_0{}^2}$ is the normalized transmission distance; x_0 is the half-width of the selected main lobe and let $x_0 = b^{-1}$. Obviously, the initial optical field envelope of the one-dimensional Airy beam is $\Phi(\xi = 0, x) = Ai(bx)\exp(ax)$, so the

Optics EXPRESS

phase profile satisfies $\phi(x) = phase[\Phi(\xi = 0, x)]$. Similarly, the phase distribution function of 2D Airy beam is $\phi(x, y) = phase[\Phi(x, y, z = 0)]$. In particular, previous research has demonstrated that the phase-only (binary phase) modulation Airy beam can be approximated quite well [33]. By the principle of geometric phase modulation, the unit cell at different positions needs to satisfy the phase condition $\varphi = \pm 2\theta$ to ensure that the circularly polarized incident light is converted into the opposite polarization state. At the same time, in the structural design, it should be considered that at least two elements are needed for the minimum sidelobe of the Airy beams to satisfy the Nyquist sampling theorem. Figure 1(a) is a schematic diagram of the 2D Airy beam distribution generated by the metasurface. The metasurface is composed of subwavelength rectangular nanopillars arranged on dielectric substrates of distinct thicknesses with an array area of 21 μm × 21 μm. When the circularly polarized light or linearly polarized light is vertically incident on the metasurface where the mode switching can be achieved by changing the temperature. At temperature of approximately 300 K, the VO_2 is in insulating state and the metasurface produces a transmitted Airy beam. At temperature above 340 K, the VO_2 is in metallic state and the metasurface produces a reflected Airy beam. The Airy beams at the upper and lower surfaces of the main lobe position will attenuate the main lobe and bend gradually with the increase of propagation distance. It is clearly observed from the picture that the optical beam is propagating in space with the two most basic properties: non-diffraction and self-bending. Figure 1(b) and (c) show the side and top views of the unit cell, respectively. The geometric and optical parameters of the nanopillars were scanned by a time-domain finite-difference solver, and the lattice constant of each cell was optimized to be $P = 340$ nm. To ensure sufficient transmission efficiency, the height of the pillar was set to be $H = 700$ nm.

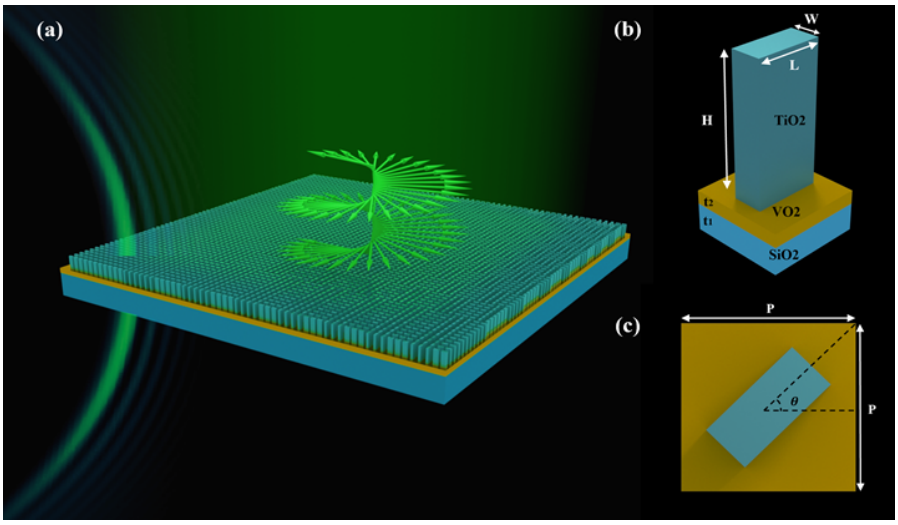

Fig. 1. Schematic diagram of the switchable all-dielectric metasurface producing a 2D Airy beam. (a) Schematic diagram of the Airy beam propagation generated by the metasurface in transmission and reflection modes. A vertically incident right-handed circularly polarized light is passing through the switchable metasurface to make a one-dimensional form of the beam trajectory. The curve is extracted from the 2D trajectory plane of the accelerated beam. As expected, the 2D Airy beam propagation trajectory is observed to remain consistent when the polarization state of the incident light is changed. (b) and (c) are the details of the unit cell, with the optimal nanopillar parameters set as $L = 237$nm, $W = 107$ nm, $t_1 = 300$ nm, and $t_2 = 100$ nm, respectively.

Optics EXPRESS

The optical properties of phase change materials vary by temperature, voltage, and various physical fields. The combination of metasurface with phase change material to achieve dynamic tunability of electromagnetic waves can increase the applicability and tunability of the metasurface [34–37]. Subsequently, priority has been given to the material aspects and the dynamic adjustment of the unit cell has been implemented by using some phase change materials to construct metasurface units. At present, the more mature materials used are graphene, VO_2, GaAs, liquid crystal, etc. The commonly used control methods are temperature control [38] and electric control [39]. VO_2 is a typical phase change material [40], which is in an insulating state at room temperature. When the temperature rises to above the phase transition temperature of $Tc = 340$K, VO_2 will undergo phase change. The lattice of VO_2 changes from a monoclinic rutile structure at low temperature to a tetragonal rutile structure at high temperature, which is externally manifested as a sudden change from the insulating state to the metallic state [41–43]. This phase transition is reversible, and the resistivity changes up to five orders of magnitude. In the visible band, when the external temperature is below the phase transition point, the permittivity of VO_2 is set as $\varepsilon = 9$. When the temperature is above the phase change point, the dispersion model is used to represent the metal as it is similar to the cold plasma. Considering the non-local characteristics of nanostructures, suitable models, such as the Debye model, Lorentz model, and Drude model, are needed to solve the dispersive medium problem [44–46]. In order to describe the electromagnetic properties of metals more accurately and fit the experimental data efficiently, a modified form of the Drude-Lorentz model was proposed in Ref. [47]. In this paper, we use the model to construct novel VO_2 metallic state materials by numerical calculations and finite difference method in time-domain (FDTD solutions, Lumerical Inc.). This hybrid model imported the data into the material library and was applicable to a wide range of frequency bands. Assuming that the number of poles of the Lorentz model is 2, the relative permittivity of VO_2 can be expressed by the following equation

$$\varepsilon_r(\omega) = \varepsilon_\infty - \frac{{\Omega_D}^2}{\omega^2 + j\gamma\omega} + \sum_{\iota=1}^{2} \chi_\iota(\omega) \tag{3}$$

$$\chi_\iota(\omega) = \frac{\Delta\varepsilon_\iota {\Omega_\iota}^2}{{\Omega_\iota}^2 - \omega^2 - j\omega 2\Gamma_\iota} + \frac{j\omega M_\iota}{{\Omega_l}^2 - \omega^2 - j\omega 2\Gamma_\iota} \tag{4}$$

where $\varepsilon_\infty = 1.03$ is the dielectric constant as the frequency tends to infinity; $\Omega_D = 1.3064e16$ is the plasma frequency; $\gamma = 1.1274e14$ is the collision frequency. The values of other parameters can be referred to in literature [48].

First, the transmission efficiency (transmittance and reflectance) and polarization conversion efficiency of a single nanopillar meta-atom with VO_2 in the insulating and metallic states were calculated using simulations in the visible band with the FDTD component in Lumerical software, respectively. To maximize the operable left- and right-handed circularly polarized light values, the polarization conversion efficiency is defined as PCE = $\frac{\mathrm{T(LCP)}}{\mathrm{T(LCP)+T(RCP)}}$ [49]. Periodic boundary conditions were used in the x and y directions, and perfectly matched layer (PML) boundary conditions were used in the z direction. As shown in Fig. 2, the spatial geometry of the single nanopillar meta-atom was continuously changed to ensure efficient transmission efficiency and to achieve perfect conversion of the polarization state. The conversion efficiency was optimized as L was varied from 230 nm to 250 nm and W from 100 nm to 120 nm, as shown in Fig. 2(a)-(d). Figure 2(a) and (b) indicate that the transmitted light through the nanopillar meta-atom exhibited high transmission and polarization conversion efficiency when VO_2 was in the insulating state. The transmission efficiency was above 95% and the polarization conversion was above 90%, which agrees with the expected results. Figure 2(c) and (d) show the reflectance and conversion of the reflected light when VO_2 was in the metallic state. By comparing Fig. 2(a) and Fig. 2(c), it can be found that the transmittance and reflectance of individual nanopillar meta-atom differ significantly in different operating modes. When VO_2 was in the metallic state, the reflected light was optically resonant in the TiO_2 waveguide, resulting in most of the energy loss so that only

Optics EXPRESS

about one third of the energy could be made full use. To verify the propagation characteristics of the Airy beams, we compared the intensity distribution of the Airy beams along the optical axis at different propagation distances based on theoretical calculations and fitted experimental simulation data when the metasurface works in transmission mode. The main lobe deflection of the Airy beams and the propagation distance satisfies the theoretical relation $u \cong \frac{\lambda^2 z^2}{16\pi^2 x_0{}^3}$ [50], and it can be seen from Fig. 2(e) that the simulated value is consistent with the theoretical curve. It is worth noting that the deflection direction of the main lobe of the 2D Airy beam was selected in the diagonal direction of the x-axis and y-axis, namely the u-direction. According to the Airy beams phase distribution equation, we designed the phase arrangement of the metasurface as shown in Fig. 2(f).

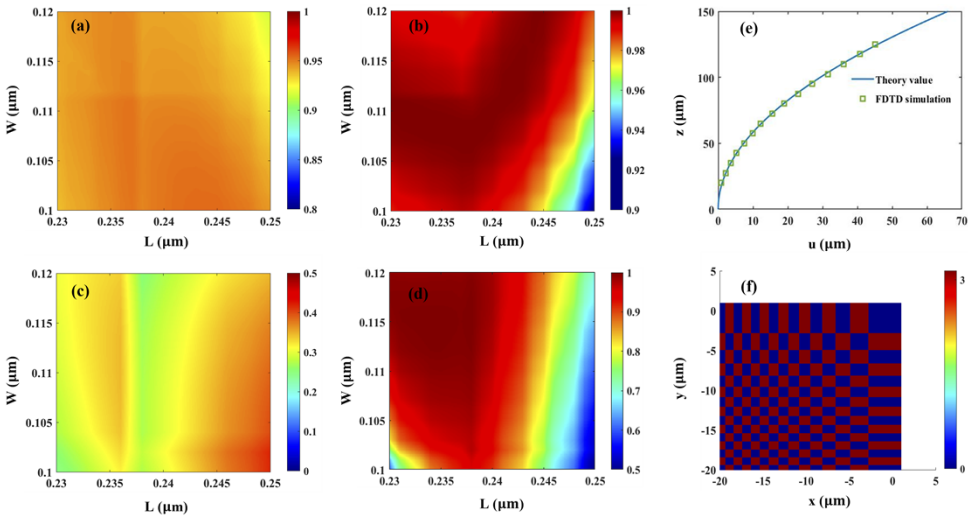

Fig. 2. The measured efficiency of the single nanopillar meta-atom and the array arrangement. (a)-(b) Simulated variation of transmittance and polarization conversion of the transmitted optical field with size when VO_2 was in the insulating phase at fixed nanopillar height. (c)-(d) The variation of reflectance and polarization conversion rate of the reflected field with cell size when VO_2 was in the metallic phase. (e) Both the simulation data (square) and the theoretical calculation equation (solid line) are shown to verify the propagation trajectory of the main lobe deflection of the Airy beam under the incidence of right-handed circularly polarized light. (f) The required phase distribution maps for different positions of the metasurface array were simulated according to the appropriately designed metasurface size.

3. Results and discussion

In this section, we proposed the generation of 2D Airy beams with mode switched by different polarized incident lights (LP, LCP, and RCP) and controlled phase transition of the VO_2 material. At the operating wavelength $\lambda = 532$ nm, the 2D phase distribution derived from the optical paraxial wave equation was combined with the numerical simulation optimization algorithm to extract the light intensity distribution along with different propagation directions. Figure 3 shows the transmission characteristics of 2D Airy beam generated by transmissive metasurface. The transverse electric field maps at different points in the z direction were retrieved sequentially from the three-dimensional (3D) far-field pattern, and the discrete longitudinal 2D electric field was reintegrated after amplification along the diagonal direction (denoted as u-direction) of the main lobe position of the transverse field map. Figure 3(a) is a longitudinal field diagram

Optics EXPRESS

for the formation of a 2D Airy beam, which consists of the main lobe and multiple sidelobes. From the diagram, it can be seen that the energy aggregation in the transmission process renders obvious attenuation, which has nondiffractive characteristics and shows lateral self-acceleration phenomenon. Figure 3(b) illustrates the transverse field distribution along the longitudinal direction from $z = 50$ μm to $z = 65$ μm. The x-y plane lattice pattern shows that most of the energy of the optical beam is intensified in the main lobe region, and that the main lobe distribution is roughly the same. In a certain range, as z increases, the energy of the main lobe is more intensified, and the light intensity is greater. It can also be seen that the main lobe light field exhibits forward acceleration characteristics along the u-direction. The field distribution shown in Fig. 3(c) is the normalized intensity distribution extracted from the cross-section along the propagation direction at the corresponding position in Fig. 3(b). In addition, Fig. 3(a) and (b) show that as the transmission distance increases, the 'tail' formed by the sidelobes of the Airy beams also increase. This is because the full width at half-maximum (FWHM) tends to increase with the increase of the propagation distance. The external manifestation is that as the waveform waist size is significantly widened, the sidelobe energy converges to the main lobe area, and the sidelobe energy is also weakened.

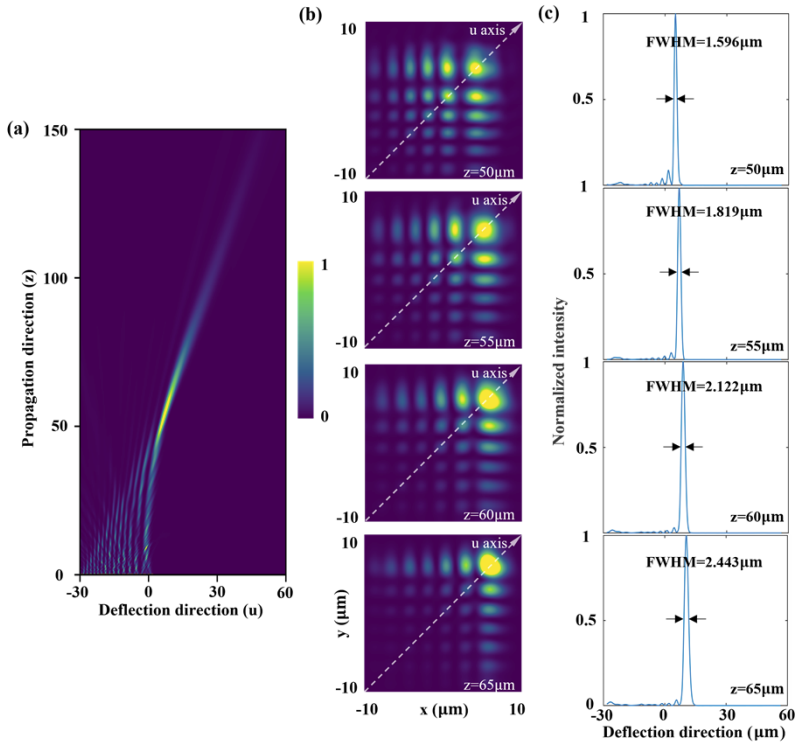

Fig. 3. The intensity distribution maps of 2D Airy beams with different planes generated in transmission mode. (a) The longitudinal field diagram of Airy beams generated under the incident conditions of left- or right-handed circularly polarized light. (b) The x-y plane field distribution recorded at the longitudinal positions of $z = 50$ μm, $z = 55$ μm, $z = 60$ μm, and $z = 65$ μm. (c) The field profile at the main lobe of the optical beam extracted based on the corresponding position in Fig. 3(b), and the measured FWHM is the normalized field intensity value.

At room temperature, as VO_2 changed from the insulating state to the metallic state, our designed metasurface would work in the reflection mode, converting the LCP (or RCP) incident

Optics EXPRESS

light into a 2D Airy beam after it passed through the nanostructures to achieve the desired design effect. Figure 4(a) and (b) show the field diagrams of the generated optical beams along different planes. As implemented in the transmission mode, the metasurface can generate and manipulate self-bending transmission and self-accelerating motion along a specific angle. If the energy transmission efficiency of the reflected Airy beams could be further improved, the metasurface would be expected to be widely used in many research fields such as the generation of microparticle manipulated plasma channels and Airy lasers. Figure 4(c) shows the normalized field intensity distribution obtained for different propagation planes ($z = 50\ \mu$m, $z = 55\ \mu$m, $z = 60\ \mu$m, and $z = 65\ \mu$m) along the u-direction. Since the scattered light generated by the reflective metasurface was not completely reflected in the TiO_2 nanopillars, a few lights would be scattered to the surrounding area. Therefore, the optical beam flatness of the 2D accelerated beam implemented by reflective metasurface was slightly weaker while FWHM was relatively larger.

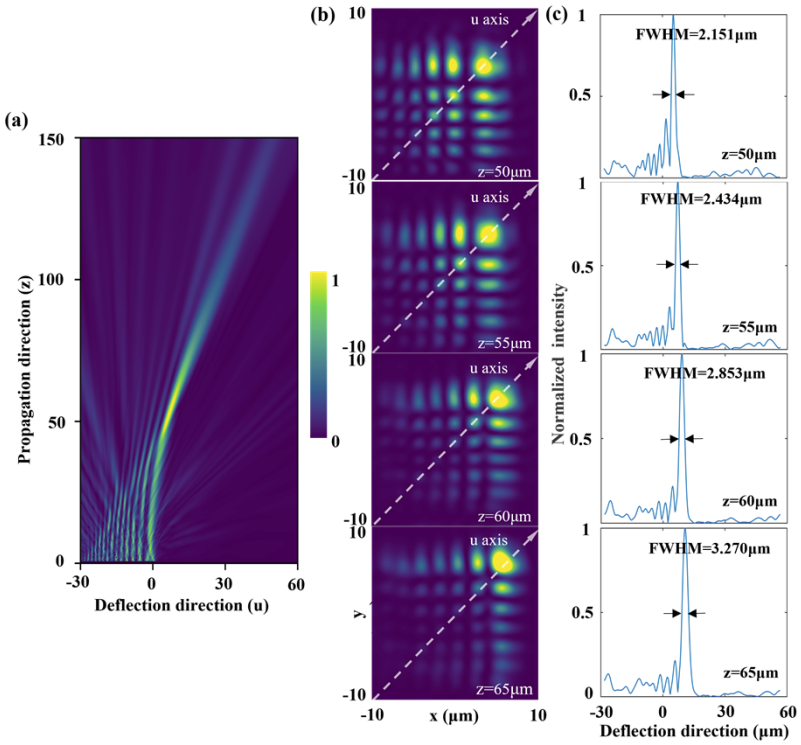

Fig. 4. Different plane field patterns of the 2D Airy beam generated by the reflective metasurface. (a) The longitudinal field diagram of the Airy beams generated under the incident conditions of left- or right-handed circularly polarized light. (b) The x-y plane field distribution of the longitudinal position recorded for different propagation planes. (c)The field profile at the main lobe of the optical beam extracted based on the position corresponding to Fig. 4 (b).

The self-healing property of nondiffractive optical beams can be explained by Babinet's criterion [51]. It has been confirmed with extensive experimental and simulation data that the self-healing behavior is one of the unique properties of accelerated beams [52]. In this paper, the self-healing properties were investigated by the blocked part of the Airy beams. When the main lobe area is blocked, as the transmission distance increases, the blocked main lobe area can be self-repaired, and the sidelobe energy flows from the surrounding area to the blocked main lobe

Optics EXPRESS

area. At this time, the main lobe will return to the unblocked area. The designed switchable metasurface was studied and confirmed based on the above-described properties. On the basis of building a complete nanopillar array, we placed spherical obstacles (the spheres are composed of different sizes and materials) at a spatial location $z = 3.3$ μm from the metasurface to study the self-healing property of the 2D Airy beams when the main lobe was obscured. Figure 5(a)-(c) show that obstacles do not affect the propagation of the Airy beam, which proves that the Airy beams generated by our designed metasurface exhibit excellent self-healing properties. As shown in Fig. 5(d) and (e), after being transmitted for a certain distance, the energy of the main lobe got close to zero in a certain spatial range, such as at $z = 10$ μm, as if it had been eliminated. From the energy distribution, according to the self-healing property of the Airy beams, the optical beams converged together during the propagation process, such as at $z = 55$ μm.

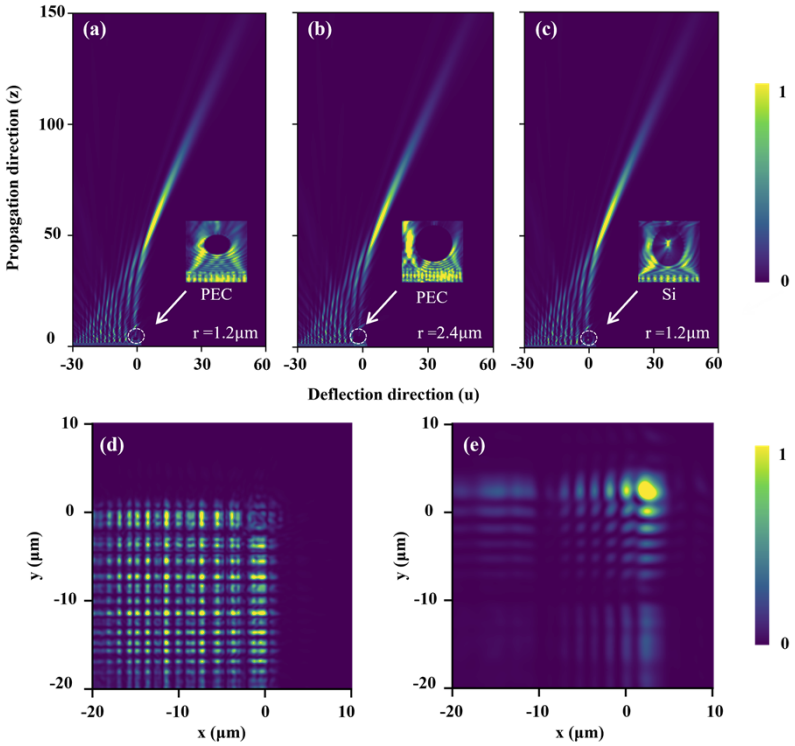

Fig. 5. Dynamic self-healing properties of 2D Airy beams under occlusion of the main lobe. (a)-(c) The obstacles were placed at $z = 3.3$ μm above the main lobe to produce a longitudinal field pattern of 2D Airy beams with increasing propagation distance and gradually decreasing energy. The spheres are made of different radii (r =1.2 μm, r = 2.4μm) and materials (perfect electric conductor, silicon). (d)-(e) The light intensity distribution generated by the transverse position recorded at $z = 10$ μm and $z = 55$ μm in the plane wave propagation direction, respectively. (Reference can be made to the upper right corner of the picture with and without the main flap for comparison.)

Below is a brief discussion about the measurement and comparison of the energy transfer efficiency of Airy beams in two adjustable working modes of the metasurface due to changing the metallic and insulating states of VO_2 via the change of ambient temperature. Numerical simulation results showed that the efficiency of the optical intensity transmission of the Airy beams was as high as 97% and 70% in the transmission and reflection modes, respectively, which was the maximum optical intensity of the generated 2D Airy beam extracted from the 3D far-field

Optics EXPRESS

pattern. The conversion efficiency is defined as the ratio of the energy of the LCP (or RCP) light obtained from the incident plane wave after metasurface conversion to the total energy of the outgoing beam. Most of the incident light passes through the metasurface in transmission mode, and about 3% of the optical beam is reflected. When the metasurface works in reflection mode, a portion of the transmitted light is lost in the structure and less than 1% of the light passes through the metasurface. It is worth noting that, compared with the reflection mode, the transmission mode of the metasurface achieved better results with higher energy utilization. To grasp the effects of different light sources on the metasurface, we chose to simulate the plane wave with differently polarized lights at the same position $z = 60$ μm passing through the metasurface in the transmission mode of operation, and the same operation can be repeated in the reflection mode.

The results are shown in Fig. 6(a)-(c). For plane waves with different polarization states, the simulated field intensity distribution changed little, except for the small difference in the energy of many sidelobes. The corresponding optical intensity conversion efficiency of LCP and RCP was 97%, and the LCP and RCP energy emitted from the LP incident light accounted for half of the total energy, respectively. Therefore, the metasurface designed in this paper is polarization sensitive and has certain selectivity and flexibility for incident light. In addition, we also verify the broadband nature of the metasurface. As shown in Fig. 6, the metasurface also produces ideal Airy beams for the wavelengths of 492 nm, 532 nm and 586 nm, respectively. And as the wavelength increases, the greater the bending of the Airy beam and the earlier the maximum light intensity appears.

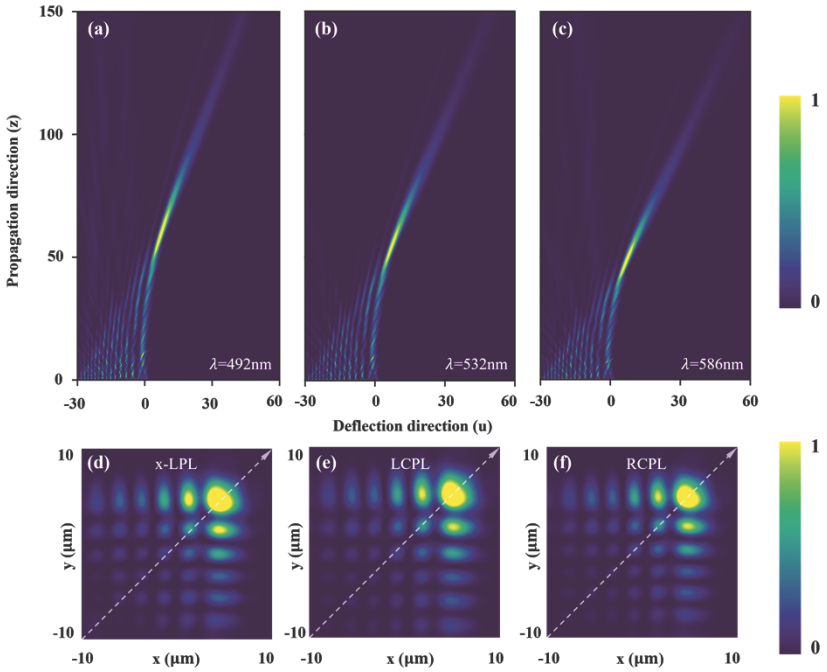

Fig. 6. (a)-(c) Diagram of the 2D Airy beam propagation trajectory at different wavelengths. Simulated (d) x-LPL, (e) left-handed circularly polarized light, (f) right-handed circularly polarized light respectively perpendicularly incident to the metasurface in the transmission mode. The intensity distribution pattern of the optical field in the x-y cross-section was generated at a distance of $z = 60$ μm from the metasurface.

Optics EXPRESS

4. Conclusion

In summary, a switchable metasurface based on VO_2 phase change materials has been designed and numerically demonstrated for the generation of 2D Airy beams in the visible range. The all-dielectric metasurface composed of TiO_2 nanopillars has exhibited many unique properties, such as high refractive index, high transmittance, and the ability to convert plane waves with arbitrary polarization into Airy beams. In this paper, the phase distribution of the 2D Airy beams has been achieved by changing the rotation angle of the nanopillars by FDTD simulation and the PB phase principle. At room temperature, when VO_2 was in an insulating state, the metasurface would produce a transmitted 2D Airy beam with high polarization conversion efficiency and transmission efficiency. At high temperature, the optimized Drude-Lorentz model was used to produce the same 2D Airy beam as the transmissive metasurface, with optical intensity conversion efficiencies of 97% and 70%, respectively. The numerical simulation results of Airy beams captured in different planes ($z = 50\ \mu$m, $z = 55\ \mu$m, $z = 60\ \mu$m, and $z = 65\ \mu$m) have verified that the Airy beam has unique characteristics such as non-diffraction, self-acceleration, and self-healing in addition to several important properties, such as polarization conversion, beam control, and switchable operating modes. Our designed metasurface is expected to be used in integrated compact optical systems such as holographic imaging.

Funding. Natural Science Foundation of Zhejiang Province (LY19F030004, LY20F050002); National Natural Science Foundation of China (61975185).

Disclosures. The authors declare no conflicts of interest.

Data availability. Data underlying the results presented in this paper are not publicly available at this time but may be obtained from the authors upon reasonable request.

References

1. J. Durnin, J. Miceli Jr., and J. H. Eberly, "Diffraction-free beams," Phys. Rev. Lett. **58**(15), 1499–1501 (1987).
2. G. A. Siviloglou and D. N. Christodoulides, "Accelerating finite energy Airy beams," Opt. Lett. **32**(8), 979–981 (2007).
3. M. V. Berry and N. L. Balazs, "Nonspreading wave packets," Am. J. Phys. **47**(3), 264–267 (1979).
4. G. A. Siviloglou, J. Broky, A. Dogariu, and D. N. Christodoulides, "Observation of accelerating Airy beams," Phys. Rev. Lett. **99**(21), 213901 (2007).
5. G. A. Siviloglou, J. Broky, A. Dogariu, and D. N. Christodoulides, "Ballistic dynamics of Airy beams," Opt. Lett. **33**(3), 207–209 (2008).
6. Z. Ren, Q. Wu, Y. Shi, C. Chen, J. Wu, and H. Wang, "Production of accelerating quad Airy beams and their optical characteristics," Opt. Express **22**(12), 15154–15164 (2014).
7. Q. Lu, S. Gao, L. Sheng, J. Wu, and Y. Qiao, "Generation of coherent and incoherent Airy beam arrays and experimental comparisons of their scintillation characteristics in atmospheric turbulence," Appl. Opt. **56**(13), 3750–3757 (2017).
8. B. Y. Wei, P. Chen, W. Hu, W. Ji, L. Y. Zheng, S. J. Ge, Y. Ming, V. Chigrinov, and Y. Q. Lu, "Polarization-controllable Airy beams generated via a photoaligned director-variant liquid crystal mask," Sci. Rep. **5**(1), 17484 (2015).
9. J. A. Davis, M. J. Mitry, M. A. Bandres, I. Ruiz, K. P. McAuley, and D. M. Cottrell, "Generation of accelerating Airy and accelerating parabolic beams using phase-only patterns," Appl. Opt. **48**(17), 3170–3176 (2009).
10. N. Voloch-Bloch, Y. Lereah, Y. Lilach, A. Gover, and A. Arie, "Generation of electron Airy beams," Nature **494**(7437), 331–335 (2013).
11. T. Vettenburg, H. I. Dalgarno, J. Nylk, C. Coll-Llado, D. E. Ferrier, T. Cizmar, F. J. Gunn-Moore, and K. Dholakia, "Light-sheet microscopy using an Airy beam," Nat. Methods **11**(5), 541–544 (2014).
12. K. Dholakia and T. Cizmar, "Shaping the future of manipulation," Nat. Photonics **5**(6), 335–342 (2011).
13. N. Yu, P. Genevet, M. A. Kats, F. Aieta, J. P. Tetienne, F. Capasso, and Z. Gaburro, "Light propagation with phase discontinuities: generalized laws of reflection and refraction," Science **334**(6054), 333–337 (2011).
14. S. Wang, P. C. Wu, V. C. Su, Y. C. Lai, C. Hung Chu, J. W. Chen, S. H. Lu, J. Chen, B. Xu, C. H. Kuan, T. Li, S. Zhu, and D. P. Tsai, "Broadband achromatic optical metasurface devices," Nat. Commun. **8**(1), 187 (2017).
15. P. C. Wu, J. W. Chen, C. W. Yin, Y. C. Lai, T. L. Chung, C. Y. Liao, B. H. Chen, K. W. Lee, C. J. Chuang, C. M. Wang, and D. P. Tsai, "Visible Metasurfaces for On-Chip Polarimetry," ACS Photonics **5**(7), 2568–2573 (2018).
16. B. J. Xu, C. Wu, Z. Y. Wei, Y. C. Fan, and H. Q. Li, "Generating an orbital-angular-momentum beam with a metasurface of gradient reflective phase," Opt. Mater. Express **6**(12), 3940–3945 (2016).
17. M. K. Chen, Y. F. Wu, L. Feng, Q. B. Fan, M. H. Lu, T. Xu, and D. P. Tsai, "Principles, Functions, and Applications of Optical Meta-Lens," Adv. Opt. Mater. **9**(4), 2001414 (2021).

Optics EXPRESS

18. Z. Sun, B. Xu, B. Wu, X. Wang, and H. Ying, "High Efficiency Focusing and Vortex Generator Based on Polarization-Insensitive Gallium Nitride Metasurface," Nanomaterials **11**(10), 2638 (2021).
19. D. Abdollahpour, S. Suntsov, D. G. Papazoglou, and S. Tzortzakis, "Spatiotemporal airy light bullets in the linear and nonlinear regimes," Phys. Rev. Lett. **105**(25), 253901 (2010).
20. S. Wang, X. Wang, and Y. Zhang, "Simultaneous Airy beam generation for both surface plasmon polaritons and transmitted wave based on metasurface," Opt. Express **25**(20), 23589–23596 (2017).
21. B. R. Wu, B. J. Xu, Z. Z. Li, P. Cheng, X. J. Xue, Z. T. Sun, J. M. Wang, Y. Z. Wang, Y. A. Zhi, L. Lin, X. G. Wang, and Y. Hao, "Metalens and vortex generator based on a planar optics metasurface," Opt. Mater. Express **11**(5), 1383–1389 (2021).
22. Z. Wu, B. Xu, M. Yan, B. Wu, P. Cheng, and Z. Sun, "Tunable terahertz perfect absorber with a graphene-based double split-ring structure," Opt. Mater. Express **11**(1), 73–79 (2021).
23. Z. C. Sun, M. Y. Yan, and B. J. Xu, "Formation of orbital angular momentum and focused beams based on chiral double-helical metamaterials," Opt. Mater. **107**, 109962 (2020).
24. Z. C. Sun, M. Y. Yan, T. E. Mupona, and B. J. Xu, "Control Electromagnetic Waves Based on Multi-Layered Transparent Metasurface," Front. Phys. **7**, 181 (2019).
25. Z. C. Sun, M. Y. Yan, and B. J. Xu, "Generation of orbital angular momentum and focused beams with tri-layer medium metamaterial*," Chin. Phys. B **29**(10), 104101 (2020).
26. R. Feng, B. Ratni, J. Yi, H. Zhang, A. de Lustrac, and S. N. Burokur, "Versatile metasurface platform for electromagnetic wave tailoring," Photonics Res. **9**(9), 1650–1659 (2021).
27. R. Feng, B. Ratni, J. Yi, K. Zhang, X. Ding, H. Zhang, A. de Lustrac, and S. N. Burokur, "Versatile Airy-Beam Generation Using a 1-Bit Coding Programmable Reflective Metasurface," Phys. Rev. Appl. **14**(1), 014081 (2020).
28. C. Zhang, S. Divitt, Q. Fan, W. Zhu, A. Agrawal, Y. Lu, T. Xu, and H. J. Lezec, "Low-loss metasurface optics down to the deep ultraviolet region," Light: Sci. Appl. **9**(1), 1–10 (2020).
29. Z. Ju, J. Wen, L. Shi, B. Yu, M. Deng, D. Zhang, W. Hao, J. Wang, S. Chen, and L. Chen, "Ultra-Broadband High-Efficiency Airy Optical Beams Generated with All-Silicon Metasurfaces," Adv. Opt. Mater. **9**(1), 2001284 (2021).
30. H. Ahmed, A. A. Rahim, M. M. Ali, and H. Maab, "Symmetric accelerating beam generation via all-dielectric metasurfaces," RSC Adv. **10**(51), 30282–30288 (2020).
31. Q. Cheng, J. Wang, L. Ma, Z. Shen, J. Zhang, X. Zheng, T. Chen, Y. Yu, D. Yu, Q. He, W. Hu, T. Li, S. Zhuang, and L. Zhou, "Achromatic terahertz Airy beam generation with dielectric metasurfaces," Nanophotonics **10**(3), 1123–1131 (2021).
32. E. Y. Song, G. Y. Lee, H. Park, K. Lee, J. Kim, J. Hong, H. Kim, and B. Lee, "Compact Generation of Airy Beams with C-Aperture Metasurface," Adv. Opt. Mater. **5**(10), 1601028 (2017).
33. A. Minovich, A. E. Klein, N. Janunts, T. Pertsch, D. N. Neshev, and Y. S. Kivshar, "Generation and near-field imaging of Airy surface plasmons," Phys. Rev. Lett. **107**(11), 116802 (2011).
34. W. J. Chen, R. Chen, Y. Zhou, and Y. G. Ma, "A Switchable Metasurface Between Meta-Lens and Absorber," IEEE Photonics Technol. Lett. **31**(14), 1187–1190 (2019).
35. F. Ding, S. M. Zhong, and S. I. Bozhevolnyi, "Vanadium Dioxide Integrated Metasurfaces with Switchable Functionalities at Terahertz Frequencies," Adv. Opt. Mater. **6**(9), 1701204 (2018).
36. J. K. Yang and H. S. Jeong, "Switchable Metasurface with VO2 Thin Film at Visible Light by Changing Temperature," Photonics **8**(2), 57 (2021).
37. L. Chen, L. Zhao, Y. Hao, W. Liu, Y. Wu, Z. Wei, N. Xu, S. Qin, X. Yang, and H. Liu, "Metasurface Spiral Focusing Generators with Tunable Orbital Angular Momentum Based on Slab Silicon Nitride Waveguide and Vanadium Dioxide (VO2)," Nanomaterials **10**(9), 1864 (2020).
38. W. J. M. Kort-Kamp, S. Kramadhati, A. K. Azad, M. T. Reiten, and D. A. R. Dalvit, "Passive Radiative "Thermostat" Enabled by Phase-Change Photonic Nanostructures," ACS Photonics **5**(11), 4554–4560 (2018).
39. F. Z. Shu, J. N. Wang, R. W. Peng, B. Xiong, R. H. Fan, Y. J. Gao, Y. M. Liu, D. X. Qi, and M. Wang, "Electrically Driven Tunable Broadband Polarization States via Active Metasurfaces Based on Joule-Heat-Induced Phase Transition of Vanadium Dioxide," Laser Photonics Rev. **15**(10), 2100155 (2021).
40. Z. W. Shao, X. Cao, H. J. Luo, and P. Jin, "Recent progress in the phase-transition mechanism and modulation of vanadium dioxide materials," NPG Asia Mater. **10**(7), 581–605 (2018).
41. N. A. Butakov, I. Valmianski, T. Lewi, C. Urban, Z. Ren, A. A. Mikhailovsky, S. D. Wilson, I. K. Schuller, and J. A. Schuller, "Switchable Plasmonic–Dielectric Resonators with Metal–Insulator Transitions," ACS Photonics **5**(2), 371–377 (2018).
42. A. S. Barker, H. W. Verleur, and H. J. Guggenheim, "Infrared Optical Properties of Vanadium Dioxide Above and Below the Transition Temperature," Phys. Rev. Lett. **17**(26), 1286–1289 (1966).
43. Q. Y. Wen, H. W. Zhang, Q. H. Yang, Y. S. Xie, K. Chen, and Y. L. Liu, "Terahertz metamaterials with VO2 cut-wires for thermal tunability," Appl. Phys. Lett. **97**(2), 021111 (2010).
44. P. T. Chen, C. H. Wang, and J. R. Ho, "A lattice Boltzmann model for electromagnetic waves propagating in a one-dimensional dispersive medium," Computers & Mathematics with Applications **65**(6), 961–973 (2013).
45. B. H. Jung, Z. C. Mei, T. K. Sarkar, and M. Salazar-Palma, "Analysis of transient wave propagation in an arbitrary frequency-dispersive media using the associated laguerre functions in the FDTD-MOD method," Microw. Opt. Technol. Lett. **54**(4), 925–930 (2012).

Optics EXPRESS

46. O. Ramadan, "Systematic wave-equation finite difference time domain formulations for modeling electromagnetic wave-propagation in general linear and nonlinear dispersive materials," Int. J. Mod. Phys. C **26**(04), 1550046 (2015).
47. J. X. Liu, Y. Jiang, L. H. Ming, W. C. Tang, and H. W. Yang, "A Drude-Two-CP-FDTD method for Drude-critical points model of metal nanofilms," Eur. Phys. J. Plus **135**(10), 805 (2020).
48. A. Vial and T. Laroche, "Description of dispersion properties of metals by means of the critical points model and application to the study of resonant structures using the FDTD method," J. Phys. D: Appl. Phys. **40**(22), 7152–7158 (2007).
49. Q. Zhou, M. Liu, W. Zhu, L. Chen, Y. Ren, H. J. Lezec, Y. Lu, A. Agrawal, and T. Xu, "Generation of Perfect Vortex Beams by Dielectric Geometric Metasurface for Visible Light," Laser Photonics Rev. **15**(12), 2100390 (2021).
50. B. R. Wu, B. J. Xu, X. G. Wang, and H. Ying, "Generation of a polarization insensitive Airy beam using an all-dielectric metasurface," Opt. Mater. Express **11**(3), 842–847 (2021).
51. Z. Bouchal, J. Wagner, and M. Chlup, "Self-reconstruction of a distorted nondiffracting beam," Opt. Commun. **151**(4-6), 207–211 (1998).
52. M. Hashemi, A. N. K. Reddy, M. Alibakhshikenari, F. Falcone, T. A. Denidni, and E. Limiti, "Stable Light Focusing by Meta-Axicons Applicable in Biosensors, Particle Trapping, Astronomical, and Imaging Devices," in 2020 IEEE Asia-Pacific Microwave Conference (APMC) (2020), pp. 354–356.